Bio-Medical Materials and Engineering 26 (2015) S1213–S1222
DOI 10.3233/BME-151418
IOS Press

Computer-aided detection of lung nodules using outer surface features

Önder Demir[a,*] and Ali Yılmaz Çamurcu[b]
[a]*Computer Engineering Department, Technology Faculty, Marmara University, 34722 Kadikoy, İstanbul, Turkey*
[b]*Computer Engineering Department, Engineering Faculty, Fatih Sultan Mehmet Vakif University, 34445 Beyoglu, İstanbul, Turkey*

Abstract. In this study, a computer-aided detection (CAD) system was developed for the detection of lung nodules in computed tomography images. The CAD system consists of four phases, including two-dimensional and three-dimensional preprocessing phases. In the feature extraction phase, four different groups of features are extracted from volume of interests: morphological features, statistical and histogram features, statistical and histogram features of outer surface, and texture features of outer surface. The support vector machine algorithm is optimized using particle swarm optimization for classification. The CAD system provides 97.37% sensitivity, 86.38% selectivity, 88.97% accuracy and 2.7 false positive per scan using three groups of classification features. After the inclusion of outer surface texture features, classification results of the CAD system reaches 98.03% sensitivity, 87.71% selectivity, 90.12% accuracy and 2.45 false positive per scan. Experimental results demonstrate that outer surface texture features of nodule candidates are useful to increase sensitivity and decrease the number of false positives in the detection of lung nodules in computed tomography images.

Keywords: Lung nodule detection, CAD systems, texture features, medical image processing, classification

1. Introduction

Lung cancer is the most widespread form of cancer, with the highest mortality rate worldwide [1]. Radiologists thus examine numerous computerized tomography (CT) scans of lungs each day. In addition to the large number of CT images, the small size of nodules and the difficulty in distinguishing them from native lung structures, such as vessels and bronchi, contribute to very long time periods necessary for the examination of CT scan images. Computer aided detection (CAD) systems can assist radiologists in the detection of lung nodules. Image intensity thresholding is a frequently used method in the preprocessing phase of image segmentation [2-4]; airway tree and vessel segmentation are also helpful methods [5-7]. Morphological image processing methods are often used to specify regions of interests (ROIs), volumes of interests (VOIs) and segmentation [8-12]. CAD systems use extracted features from ROIs and VOIs to determine nodule or non-nodule candidate. Statistical, histogram, morphological and textural features can be used in the classification

* Address for correspondence: Önder Demir, Computer Engineering Department, Technology Faculty, Marmara University, 34722 Kadikoy, İstanbul, Turkey. Tel.: +90 (216) 3365770/1226; Fax: +90 (216) 337 89 87; E-mail: odemir@marmara.edu.tr.

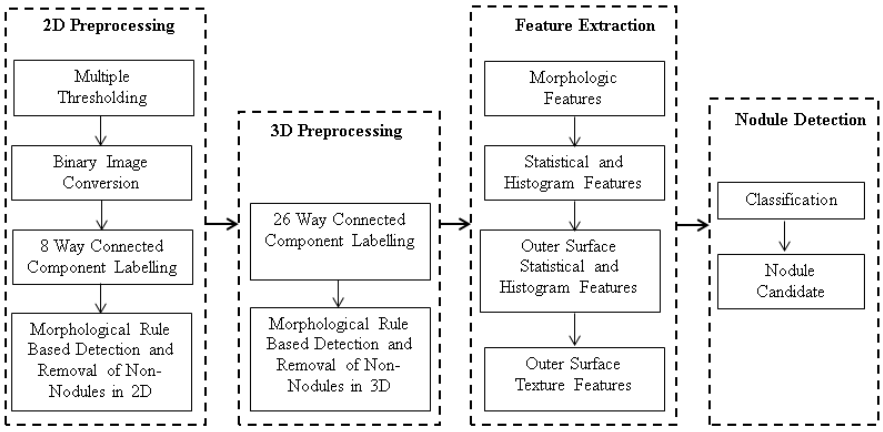

Fig. 1. Block diagram of the CAD system.

phase [13-16], as well as rule-based approaches [17, 18], artificial neural networks [19, 20], genetic algorithms [21], clustering algorithms [22], and support vector machines (SVM) [23-25].

In this study, a CAD system was developed with the aim of reducing the time radiologist required to examine CT scans, as well as reducing the margin of error through the use of outer surface features.

2. Developed CAD system

The block diagram of the CAD system is presented in Figure 1. During the preprocessing phase, unwanted forms are eliminated from the CT images and the relevant volumes are identified. During the feature extraction phase, the features of the VOI are calculated and recorded in a feature matrix. Next, the features of the VOIs are classified, and a nodule candidate is identified.

2.1. Preprocessing phase

The preprocessing phase of a CAD system serves to enhance the image and to identify the ROI or VOI by means of procedures performed on the actual medical images. The developed CAD system has both 2D and 3D preprocessing phases.

2.1.1. Gray level ıntensity thresholding and conversion to binary image

In the 2D preprocessing phase, a multiple thresholding method was applied to threshold the pixel value range which constitutes a form. The lower limit is designated the minimum intensity threshold, and the upper limit is referred to as the maximum intensity threshold. The pixel values between these two threshold values constitute the ROI, in which nodules may be present. Following the image thresholding process, CT images are converted into binary images [26-28].

2.1.2. Adjacency examination and labeling

The technique of conducting an adjacency examination on binary images is frequently used to identify abnormal forms in numerous image processing applications. A procedure can be performed on the actual image using the coordinates of the identified forms on the binary image as a result of the adjacency examination. Conducting an adjacency examination on binary images involves the

Fig. 2. (a) Binary image matrix; (b) adjacencies; (c) labeled adjacencies.

identification of values of 1 present on adjacent pixels. For all pixels with a value of 1, the adjacencies of every pixel in all 8 directions are evaluated; this process is repeated for every adjacent pixel with a value of 1 [29, 30]. When the adjacency examination is performed for a minimum number of adjacencies, small forms are ignored in order to simplify the calculation; the identified adjacencies are specified on a label matrix. This label matrix is convenient for morphological feature extraction procedures, performed on adjacencies for which the label matrices have been identified. The coordinates of the label numbers included in the label matrix can also be accessed on the actual image in order to perform feature extraction on the basis of intensity values. Figure 2 displays an adjacency identification performed due to the results of an adjacency examination with a minimum of 4 adjacencies. The actual binary image matrix is represented in Figure 2(a), while Figure 2(b) demonstrates adjacencies that were identified, both labeled and unlabeled. The label matrix created as a result of that particular adjacency examination is presented in Figure 2(c).

2.1.3. Rule-based detection of non-nodules in 2D preprocessing

Lung nodules are generally spherical in form; when lung CT images are examined in 2D, the circular forms should be identified in order to detect the nodules. The spherical forms are examined on a 3D basis. In order to enhance the performance of the CAD system, the forms on a lung CT slice image which are not circular in 2D are removed.

To perform this procedure, a rule-based method is applied on the thresholded slice images. The minimum distance and maximum distance thresholds are used to detect circular forms of a minimum size. The adjacencies of each pixel in eight directions which may represent a region of interest based on the intensity value are examined. Forms with adjacencies found by examination to be below the minimum distance threshold or greater than the maximum distance threshold in any direction are excluded; the numbers and pixel coordinates of slices that include the forms which cannot be regions of interest are recorded. This information will later be used in the removal stages of non-spherical volumes of interest in the 3D preprocessing phase. The resulting images of the procedures involved in gray level thresholding and the subsequent conversion to binary images as applied to lung CT slices are presented in Figures 3(a) and 3(b). The regions of interests identified as a result of the 2D preprocessing are shown in Figure 3(c).

2.2. 3D preprocessing phase

Each pixel with a value of 1 located in the image matrix during the adjacency examination is subjected to an examination of adjacency in 26 directions; these 26 adjacent forms are comprised of the 8 adjacent pixels in the same slice as the examined pixel, 9 adjacent pixels in the previous slice to

Fig. 3. (a) CT image; (b) binary image; (c) ROIs after 2D preprocessing.

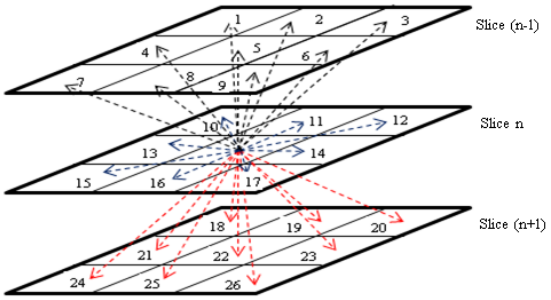

Fig. 4. Adjacency examination in 26 directions.

E = label number of the volume of interest;
Ki = first section no;
Km = section where the field is the widest;
Ks = last section no;
If the field of *E* is generally not increased in sections between *Ki* and *Km*,
Not a nodule candidate
Or if the field of *E* is generally not decreased in sections between *Km* and *Ks*
E is not a nodule candidate
Else *E* is a nodule candidate

Fig. 5. Pseudo code for identifying spherical forms in a CT scan.

the examined pixel, and 9 adjacent pixels in the following slice of the examined pixel. Figure 4 shows the examined pixel and its adjacent forms in 26 directions. An adjacent pixel with a value of 1 identified in any direction is labeled with the same label number, and is subjected to an adjacency examination in 26 directions. This procedure continues until all pixels are labeled.

The circular forms are identified in a rule-based approach during the image preprocessing phase. The first rules applied are related to the area, or the number of pixels in the volume of interest in its respective slice. The area of the structures in the spherical form gradually increases from the slice in which they were first observed towards the slices in which the middle sections of the form are located.

It is observed that the area gradually decreases from these slices towards the final slices the structure is imaged. A rule which controls the area in consecutive slices has been set in order to remove structures such as vessels, the areas of which do not change at a specific rate. The lung nodules may also have an ellipsoidal form. Therefore, the forms in which the field increases are first fixed in some slices and then begin to decrease, are not excluded based on these rules. A pseudo code for identifying the spherical forms in a CT scan is presented in Figure 5.

2.3. Feature extraction phase

The developed CAD system extracts four different groups of features from a VOI: morphological features, statistical and histogram features, outer surface statistical and histogram features, and outer surface textural features. These features are listed in Table 1. Morphological features are observed by means of measurements and calculations determined by the shape of the VOI. In this phase, seven features are extracted. The statistical and histogram features are determined by the values of voxels in the VOIs and the statistical calculations made based on these values, made on the basis of pixel values in actual images [31-33]. The outer surface of a VOI is identified on the label matrix by detecting the coordinates of the voxels constituting the VOI located on the delineations of the VOI in the CT slice images.

Analysis of textural features provides characteristic data related to textural image processing applications; Haralick's Gray level Co-occurrence Matrix is a statistical method widely used for textural analysis. The outer surface textural features are calculated using the Gray Level Co-occurrence Matrix (GLCM). GLCM is a two-dimensional matrix in which the frequency of occurrence of gray level combinations is plotted based on an examination of the binary adjacencies of pixels constituting the textural image [34-39].

The GLCM is created according to the adjacency relationship of two pixels. Of the pixels examined, the first is called the reference pixel, and the second is called the adjacent or target pixel. The direction of the adjacency examination is important in creating the GLCM. During the process of creating the

Table 1

Extracted features

Number	Morphological Features	Number	Statistical and Histogram Features
1	Volume	1	Mean
2	Minimum Axis Length (MinA)	2	Maximum Pixel Value
3	Maximum Axis Length (MaxA)	3	Minimum Pixel Value
4	MinA / MaxA	4	Most Frequent Pixel Value
5	Equivalent Radius	5	Varience
6	Sphericity	6	Standard Deviation
7	Compactness	7	Skewness
		8	Kurtosis
Number	Outer Surface Statistical and Histogram Features	Number	Outer Surface Texture Surface
1	Mean	1	Contrast
2	Maximum Pixel Value	2	Energy
3	Minimum Pixel Value	3	Entropy
4	Most Frequent Pixel Value	4	Homogenity
5	Varience	5	Moment
6	Standard Deviation		
7	Skewness		
8	Kurtosis		

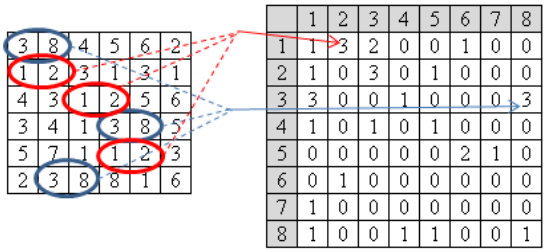

Fig. 6. Calculation of a GLCM

Table 2

Data of training and test groups

Group	Number of Patients	Number of Slices	Number of Nodules	Number of Non-Nodule Structures
Training	100	13547	572	1314
Test	100	14211	609	-

GLCM, the examinations may also be performed on the basis of the reference pixel's adjacencies in 8 directions. On the image matrix, all pixels from the top left corner to the bottom right corner are examined alternately as reference pixels. Figure 6 demonstrates the creation of GLCM.

2.4. Classification phase

In the CAD system, the support vector machine (SVM) was used as a classification algorithm, based on the statistical learning theory presented in by [40, 41]. Particle swarm algorithm (PSO) is an optimization technique presented in 1995 by [42, 43]. The PSO algorithm was developed for the optimization of functions that are not continuously linear. The support vector machine used in the study was optimized by the particle swarm algorithm [44-46].

3. Experimental studies with the CAD system

The CT images used to measure the performance of the developed CAD system were taken from the Lung Image Database Consortium—Image Database Research Initiative (LIDC – IDRI) image data set in the Cancer Imaging Archive (TCIA) archive. This database was developed by the LIDC formed by the National Cancer Institute (NCI). The LIDC-IDRI database includes 1018 CT scan results of 1010 patients, consisting of a total of 244,527 slices obtained by CT scan [47, 48]. In this study, 27,758 images of 200 patients were selected at random from the LIDC-IDRI collection. Slice thicknesses of selected scans were 1 mm. 100 patients were used for the training of the classification algorithm, while the images belonging to the remaining 100 patients were used for the test. The data pertaining to the training and test groups is presented in Table 2.

3.1. Implementation of experiments

The experiments of the CAD system were performed using two different groups of extracted features in order to determine their impact on test performance. In the first group, statistical, histogram-related features were included, while in the second group outer surface statistical features

added. In the third group, the outer surface textural features were added to other features. The classification algorithm was trained using data of 100 patients in the training group. The performance of the CAD system was measured on with the images of 100 patients in the test group.

The CAD system identified 570 out of 609 real nodules in the first group on the basis of features. The CAD system made correct detections for 1622 of 1983 non-nodule structures. The CAD system identified 593 out of 609 real nodules in the second group on the basis of features. The CAD system made correct detections for 1713 of 1983 non-nodule structures. The CAD system achieved greater success when the classification algorithm was trained through the addition of the outer surface textural features; in these experiments, the average number of false positive (FP) results per patient was 2.7. The CAD system identified 597 of 609 nodules correctly in these experiments. It made correct detections for 1748 of 1983 non-nodule structures; in these experiments, the rate of false positive (FP) results per patient was reduced to 2.45. The performance rates of the CAD system can be seen in Table 3. ROC curves of all experiment types are shown in Figure 7.

Table 3

Experimental results

Status of Features	Sensitivity	Selectivity	Accuracy	FP
Morphological, statistical and histogram features	93.60%	81.80%	85.07%	3.75
+ Outer surface statistical and histogram features	97.37%	86.38%	88.97%	2.7
+ Outer surface textural features	98.03%	87.71%	90.12%	2.45

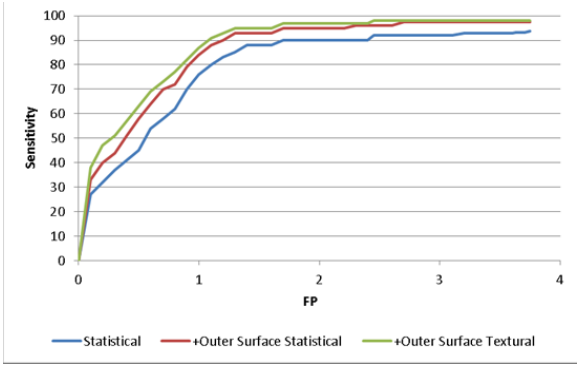

Fig. 7. ROC Curves of the CAD system.

Table 4

Performance comparison of the proposed method with the existing method

Work	Dataset	Features	Sensitivity	FP/Scan
[49]	50 Scans	Morphological, statistical	89%	7.3
[50]	84 Scans	3D Morphological, statistical	97% 88%	6.1 2.5
[51]	112 Scans	Morphological, 2D textural	85.91%	1.82
[52]	28 Scans	Textural	90.6%	1.17
[21]	-	2D, 3D Morphological, statistical	94.1%	5.45
[53]	42 Scans	Morphological, 3D shape Index	95.9%	0.22
[54]	-	Surface Statistical	97.5%	6.76
Our study	100 Scans	2D, 3D Morphological, statistical, Outer surface statistical and textural features	98.03%	2.45

Table 4 compares proposed method for nodule detection with recent studies. We selected 8 CAD schemes which are using similar methods and datasets. The performance of our method is similar to or better than other methods. The summary of comparison can be seen in Table 4.

4. Conclusion

In this study, a CAD system capable of extracting and classifying the morphological, statistical and histogram-related, and outer surface texture features of lung nodules was developed. The performance of the CAD system was measured without including the outer surface statistical and textural features; in these experiments, the FP rate of 3.75 per patient with a sensitivity of 93.6% was achieved with the CAD system. Then, performance of the CAD system was measured with including outer surface statistical features. In these experiments, the FP rate of 2.7 per patient with a sensitivity of 97.37% was achieved with the CAD system. When the performance was measured by including the outer surface textural features, the CAD system had a greater rate of success; while the sensitivity of these experiments was 98.03%, the FP rate per patient dropped to 2.45. The nodules which could not be detected by the developed CAD system were examined. As part of this examination, it was determined that the nodules adjoining the lung wall could not be detected by the CAD system. Furthermore, the nodules for which the gray level was outside the threshold values could also not be detected by the CAD system.

As a result of performed experiments, it was demonstrate that the outer surface textural features of lung nodules are distinctive. These features increase the sensitivity of the CAD system and decrease the FP number per CT scan. The success achieved by the CAD system demonstrates that it can be effectively used in clinical studies.

References

[1] Cancer Incidence in Five Continents, Available at: http://ci5.iarc.fr/, last accessed: Oct. 2nd, 2015.
[2] S.G. Armato III, M.L. Giger and H. MacMahon, Automated detection of lung nodules in CT scans: preliminary results, Medical Physics **28** (2001), 1552.
[3] S. Diciotti, et al., 3-D segmentation algorithm of small lung nodules in spiral CT images, IEEE Transactions on Information Technology in Biomedicine **12** (2008), 7-19.
[4] I. Sluimer, et al., Computer analysis of computed tomography scans of the lung: a survey, IEEE Transactions on Medical Imaging **25** (2006), 385-405.
[5] T. Jia, H. Zhang and H. Meng, A novel lung nodules detection scheme based on vessel segmentation on CT images, Bio-Medical Materials and Engineering **24** (2014), 3179-3186.
[6] W. Tan, et al., A novel method for automated segmentation of airway tree, 2012 24th Chinese Control and Decision Conference (CCDC), Taiyuan, 2012, pp. 976-979.
[7] S. Ukil and J.M. Reinhardt, Smoothing lung segmentation surfaces in 3 D X-ray CT images using anatomic guidance, Proceedings of SPIE **5370** (2004), 1066-1075.
[8] K. Awai, et al., Pulmonary nodules at chest CT: Effect of computer-aided diagnosis on radiologists' detection performance, Radiology **230** (2004), 347-352.
[9] T. Ezoe, et al., An automatic detection method of lung cancers including ground glass opacities from chest X-ray CT images, Proceedings of SPIE **4684** (2002), 1672-1680.
[10] C. Fetita, et al., 3D automated lung nodule segmentation in HRCT, Medical Image Computing and Computer-Assisted Intervention-MICCAI 2003 **2878** (2003), 626-634.
[11] J. Lai and Q. Wei, Automatic lung fields segmentation in CT scans using morphological operation and anatomical information, Bio-Medical Materials and Engineering **24** (2014), 335-340.
[12] J.R. Yong, et al., Automatic segmentation of juxta-pleural tumors from CT images based on morphological feature

analysis, Bio-Medical Materials and Engineering **24** (2014), 3137-3144.
[13] S. Ozekes and A.Y. Camurcu, Automatic lung nodule detection using template matching, Advances in Information Systems **4243** (2006), 247-253.
[14] W.C. Shen, Y.H. Yu and C.H. Chuang, Computer aided diagnosis for pulmonary nodule on low-dose computed tomography (LDCT) using density features, 2011 Eighth International Conference on Computer Graphics, Imaging and Visualization (CGIV), Singapore, 2011, pp. 166-169.
[15] H. Wang, et al., Multilevel binomial logistic prediction model for malignant pulmonary nodules based on texture features of CT image, European Journal of Radiology **74** (2010), 124-129.
[16] L. Yue, L. Jie and M. Lingjun, Suspected pulmonary nodule detection algorithm based on morphology and gray entropy, 2011 IEEE International Conference on Computer Science and Automation Engineering (CSAE), 2011.
[17] S. Ozekes and A.Y. Camurcu, Rule based detection of lung nodules ın CT ımages, IU-Journal of Electrical & Electronics Engineering **6** (2006), 61-67.
[18] J. Tong, W. Ying and W.C. Dong, A lung cancer lesions dectection scheme based on CT image, 2010 2nd International Conference on Signal Processing Systems (ICSPS), 2010.
[19] Z. Shi, et al., A new method based on MTANNs for cutting down false-positives: An evaluation on different versions of commercial pulmonary nodule detection CAD software, Bio-Medical Materials and Engineering **24** (2014), 2839-2846.
[20] X. Zhang, et al., Computerized detection of pulmonary nodules using cellular neural networks in CT images, Proceedings of SPIE **5370** (2004), 30-41.
[21] W.J. Choi and T.S. Choi, Genetic programming-based feature transform and classification for the automatic detection of pulmonary nodules on computed tomography images, Information Sciences **212** (2012), 57-58.
[22] J. Gao, et al., Classification of normal and cancerous lung tissues by electrical impendence tomography, Bio-Medical Materials and Engineering **24** (2014), 2229-2241.
[23] J.R.F. da Silva Sousa, et al., Methodology for automatic detection of lung nodules in computerized tomography images, Computer Methods and Programs in Biomedicine **98** (2010), 1-14.
[24] Y. Liu, et al., A method of pulmonary nodule detection utilizing multiple support vector machines, International Conference on Computer Application and System Modeling **10** (2010), 118-121.
[25] Y. Liu, et al., A study of pulmonary nodule detection in three-dimensional thoracic CT scans, Second International Conference on Computer Modeling and Simulation **1** (2010), 481-484.
[26] B. Golosio, et al., A novel multithreshold method for nodule detection in lung CT, Medical Physics **36** (2009), 3607.
[27] N. Otsu, A threshold selection method from gray-level histograms, Automatica **11** (1975), 23-27.
[28] M. Sezgin and B. Sankur, Survey over image thresholding techniques and quantitative performance evaluation, Journal of Electronic Imaging **13** (2004), 146-168.
[29] P.A. Devijver, Connected Components in Binary Images: The Detection Problem, John Wiley & Sons, Inc., New York, 1984.
[30] L. Di Stefano and A. Bulgarelli, A simple and efficient connected components labeling algorithm, Proceedings. International Conference on Image Analysis and Processing, Venice, 1999, pp. 322-327.
[31] T. Messay, R.C. Hardie and S.K. Rogers, A new computationally efficient CAD system for pulmonary nodule detection in CT imagery, Medical Image Analysis **14** (2010), 390.
[32] D.S. Paik, et al., Surface normal overlap: A computer-aided detection algorithm with application to colonic polyps and lung nodules in helical CT, IEEE Transactions on Medical Imaging **23** (2004), 661-675.
[33] R.N. Strickland, Image-Processing Techniques for Tumor Detection, Marcel Dekker Inc., New York, 2002.
[34] R.M. Haralick, Statistical and structural approaches to texture, Proceedings of the IEEE **67** (1979), 786-804.
[35] R.M. Haralick, K. Shanmugam and I.H. Dinstein, Textural features for image classification, IEEE Transactions on Systems, Man and Cybernetics **6** (1973), 610-621.
[36] J.R. Parker, Algorithms for Image Processing and Computer Vision, Wiley Publishing, New York, 2010.
[37] M. Tuceryan and A.K. Jain, Texture analysis, Handbook of Pattern Recognition and Computer Vision, 1993.
[38] X. Xie, A review of recent advances in surface defect detection using texture analysis techniques, Electronic Letters on Computer Vision and Image Analysis **7** (2008), 1-22.
[39] L.S. Davis, M. Clearman and J.K. Aggarwal, A comparative texture classification study based on generalized cooccurrence matrices, 1979 18th IEEE Conference on Decision and Control including the Symposium on Adaptive Processes **1** (1979), 71-78.
[40] B.E. Boser, I.M. Guyon and V.N. Vapnik, A training algorithm for optimal margin classifiers, Proceedings of the Fifth Annual Workshop on Computational Learning Theory **5** (1992), 144-152.
[41] V. Vapnik, The Nature of Statistical Learning Theory, Springer, New York, 1999.
[42] R. Eberhart and J. Kennedy, A new optimizer using particle swarm theory, Proceedings of the Sixth International

Symposium on Micro Machine and Human Science, Nagoya, 1995, pp. 39-43.
[43] J. Kennedy and R. Eberhart, Particle swarm optimization, IEEE International Conference on Neural Networks, Perth, 1995, pp. 1942-1948.
[44] M.J. Abdi, S.M. Hosseini and M. Rezghi, A novel weighted support vector machine based on particle swarm optimization for gene selection and tumor classification, Computational and Mathematical Methods in Medicine **2012** (2012), 320698.
[45] C.L. Huang and J.F. Dun, A distributed PSO–SVM hybrid system with feature selection and parameter optimization, Applied Soft Computing **8** (2008), 1381-1391.
[46] X. Li, S. Yang and J. Qi, A new support vector machine optimized by improved particle swarm optimization and its application, Journal of Central South University of Technology **13** (2006), 568-572.
[47] S.G. Armato III, et al., The lung ımage database consortium (LIDC) and ımage database resource ınitiative (IDRI): A completed reference database of lung nodules on CT scans, Medical Physics **38** (2011), 915.
[48] M.F. McNitt-Gray, et al., The lung ımage database consortium (LIDC) data collection process for nodule detection and annotation, Academic Radiology **14** (2007), 1464.
[49] M. Keshani, et al., Lung nodule segmentation and recognition using SVM classifier and active contour modeling: A complete intelligent system, Computers in Biology and Medicine **43** (2013), 287-300.
[50] D. Cascio, et al., Automatic detection of lung nodules in CT datasets based on stable 3D mass–spring models, Computers in Biology and Medicine **42** (2012), 1098-1109.
[51] A.O. de Carvalho Filho, et al., Automatic detection of solitary lung nodules using quality threshold clustering, genetic algorithm and diversity index, Artificial Intelligence in Medicine **60** (2014), 165-177.
[52] A.M. Santos, et al., Automatic detection of small lung nodules in 3D CT data using Gaussian mixture models, Tsallis entropy and SVM, Engineering Applications of Artificial Intelligence **36** (2014), 27-39.
[53] S. Saien, A.H. Pilevar and H.A. Moghaddam, Refinement of lung nodule candidates based on local geometric shape analysis and Laplacian of Gaussian kernels, Computers in Biology and Medicine **54** (2014), 188-198.
[54] W.-J. Choi and T.-S. Choi, Automated pulmonary nodule detection based on three-dimensional shape-based feature descriptor, Computer Methods and Programs in Biomedicine **113** (2014), 37-54.